

pubs.acs.org/est Article

# Ozone Production Efficiencies in the Three Largest United States **Cities from Airborne Measurements**

Wyndom S. Chace, Caroline Womack, Katherine Ball, Kelvin H. Bates, Birger Bohn, Matthew Coggon, John D. Crounse, Hendrik Fuchs, Jessica Gilman, Georgios I. Gkatzelis, Christopher M. Jernigan, Gordon A. Novak, Anna Novelli, Jeff Peischl, Ilana Pollack, Michael A. Robinson, Andrew Rollins, Nell B. Schafer, Rebecca H. Schwantes, Morgan Selby, Aaron Stainsby, Chelsea Stockwell, Rose Taylor, Victoria Treadaway, Patrick R. Veres, Carsten Warneke, Eleanor Waxman, Paul O. Wennberg, Glenn M. Wolfe, Lu Xu, Kristen Zuraski, and Steven S. Brown\*



Cite This: Environ. Sci. Technol. 2025, 59, 13306-13318



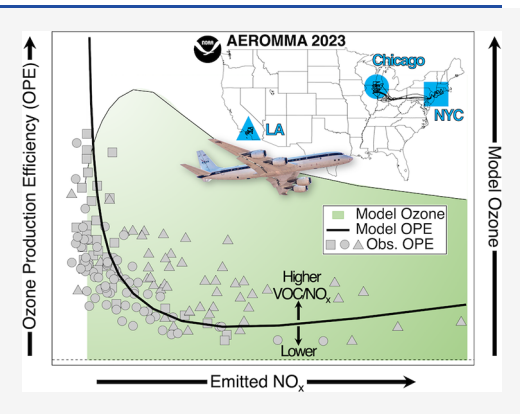
**ACCESS** 

Metrics & More

Article Recommendations

Supporting Information

ABSTRACT: Despite ongoing reductions in emissions of ozone  $(O_3)$  precursors, nitrogen oxides  $(NO_x = NO + NO_2)$  and volatile organic compounds (VOCs), the three largest urban areas in the United States — New York City (NYC), Chicago, and Los Angeles (LA) — continue to exceed national air quality standards for  $O_3$ . Airborne measurements during the 2023 Atmospheric Emissions and Reactions Observed from Megacities to Marine Areas (AEROMMA) campaign investigated nonlinear O<sub>3</sub> photochemistry in these cities. We report mean ozone production efficiency (OPE), the enhancement ratio of  $O_x$  (=  $O_3$  +  $NO_2$ ) to  $NO_x$  oxidation products, of 9  $\pm$  4 (1 $\sigma$ ), 6  $\pm$  3, and 6  $\pm$  3 ppbv ppbv<sup>-1</sup> in NYC, Chicago, and LA, respectively. Compared to historical values, OPE has increased in NYC but remains constant in LA. We find that OPE during AEROMMA has a nonlinear, inverse relationship with total reactive nitrogen (NO<sub>w</sub> a proxy for initial NO<sub>x</sub>) and a positive correlation with the nonmethane VOC to NO, enhancement ratio. A zero-dimensional photochemical model supports these observed OPE depend-



ences on NO<sub>x</sub> and VOCs and shows that OPE is a distinct metric from total O<sub>3</sub> production that is informative to the development of O<sub>3</sub> pollution control strategies. We find that OPE values have higher variability, and a larger increase with NO<sub>2</sub> emissions reductions, in areas that experience NO<sub>x</sub>-sensitive rather than NO<sub>x</sub>-saturated O<sub>3</sub> photochemistry; nonetheless, NO<sub>x</sub> reductions under NO<sub>x</sub>sensitive conditions still reduce total O<sub>3</sub> production despite the corresponding increase in OPE.

KEYWORDS: tropospheric ozone, ozone production efficiency, urban air quality, air pollution, megacities

## 1. INTRODUCTION

The majority of the global population resides in urban areas, with 13% of urban dwellers living in megacities (population > 10 million) as of 2018. Poor urban air quality is a leading threat to human health that causes millions of annual premature deaths worldwide; 2,3 with projections for continued urbanization and population growth, an increasing number of people will experience the impacts of urban air pollution in the coming decades. One major pollutant that degrades air quality is tropospheric ozone (O<sub>3</sub>), which forms photochemically from primary emissions of nitrogen oxides ( $NO_x = NO_2 + NO$ ) and volatile organic compounds (VOCs). In the United States (US) and Europe, substantial decreases in urban O<sub>3</sub> pollution have been achieved over the past decades through the mitigation of NO<sub>x</sub> emissions.<sup>4,5</sup> For the largest urban areas in the US, however, reductions in O<sub>3</sub> pollution have stagnated in recent years despite continually decreasing national NO<sub>x</sub> emissions.<sup>6,7</sup> Recent work has shown that as motor vehicle VOC emissions

continue to decline,<sup>8</sup> biogenic VOCs,<sup>9-11</sup> the class of VOCs known as volatile chemical products (VCPs), 12,13 cooking VOCs, 14 and asphalt VOCs 15 have an increasingly important contribution to O<sub>3</sub> photochemistry. 16 Other emission sources, such as increasing oil and gas development 17-20 and wildfire activity,  $^{21-24}$  have also affected recent trends in urban  $O_3$ . This changing emissions landscape may impact the photochemical regime in which urban O<sub>3</sub> production occurs. It is well-known that  $O_3$  production and abundances depend nonlinearly on NO. and VOCs. 25-27 Reactions R1-R6 are a partial list of the

Received: February 13, 2025 Revised: June 3, 2025 Accepted: June 4, 2025 Published: June 24, 2025





reactions discussed in this work, where R represents an organic constituent and M is an inert third body.

$$NO_2 + hv + O_2 \rightarrow NO + O_3 \tag{R1}$$

$$NO + O_3 \rightarrow NO_2 + O_2 \tag{R2}$$

$$NO + RO_2 \rightarrow NO_2 + RO \tag{R3a}$$

$$NO + RO_2 + M \rightarrow RONO_2 + M \tag{R3b}$$

$$NO + HO_2 \rightarrow NO_2 + OH \tag{R4}$$

$$RO + O_2 \rightarrow R = O + HO_2 \tag{R5}$$

$$NO_2 + OH \rightarrow HNO_3$$
 (R6)

In a  $NO_x$ -sensitive regime, radical propagation reactions (*e.g.*, Reactions R3a and R4) dominate  $O_3$  photochemistry and therefore  $NO_x$  emissions reductions decrease  $O_3$  production while VOC emissions reductions have little to no effect on  $O_3$ . In contrast,  $NO_x$  radical termination reactions (*e.g.*, Reactions R3b and R6) govern  $O_3$  photochemistry in a  $NO_x$ -saturated regime, resulting in increased  $O_3$  production with decreasing  $NO_x$  emissions or increasing VOC emissions.

A common metric in the  $O_3$  photochemistry literature is the ozone production efficiency (OPE), a concept introduced by Liu et al. (1987) that quantifies the number of  $O_3$  molecules produced per emitted and subsequently oxidized  $NO_x$  molecule. These  $NO_x$  termination products, such as nitric acid (HNO<sub>3</sub>), acyl peroxy nitrate (PAN), or organic nitrates, are collectively termed  $NO_z$  (total reactive nitrogen,  $NO_y$ , minus  $NO_x$ ). The conventional definition of OPE from observations is the slope of the linear regression of measured  $O_3$  against  $NO_z^{29,30}$  To account for the rapid daytime interconversion between  $NO_2$  and  $O_3$  as represented by Reactions R1 and R2, it is useful to replace  $O_3$  with odd oxygen, or  $O_x$  (=  $NO_2$  +  $O_3$ ), in OPE calculation.  $^{31,32}$  We calculate OPE in this work as the slope of  $O_x$  versus  $NO_z$  (eq 1), where  $\Delta$  indicates the enhancement above background.

$$OPE = \frac{\Delta O_x}{\Delta NO_z} = \frac{\Delta (O_3 + NO_2)}{\Delta (NO_y - NO_x)}$$
(1)

An observation-derived OPE is an integrated metric that represents the cumulative O<sub>3</sub> photochemistry in an air parcel; physical processes such as mixing, deposition, dilution, and fresh emissions can complicate its interpretation.<sup>33</sup> Photochemical modeling, when paired with observations, can parse the impacts of chemical and physical processes on OPE. Model OPE calculated from the ratio of the O<sub>3</sub> production rate to the NO<sub>x</sub> loss rate,  $P(O_3)/L(NO_x)$ , gives an instantaneous measure of OPE,<sup>34</sup> while other methods such as temporal averaging of instantaneous OPE<sup>35</sup> or calculation of modeled plume enhancements above background<sup>33,36</sup> provide a cumulative modeled OPE that is comparable to empirical values. As indicated by the definitions above, OPE is a distinct metric from total O<sub>3</sub> mixing ratio or O3 production rate; the latter are the focus of many urban  $O_3$  sensitivity analyses. <sup>37,38</sup> An OPE modeled as  $P(O_3)$ /  $L(NO_x)$  can be considered against  $P(O_3)$ , as both represent instantaneous quantities, whereas an observation-based or cumulative modeled OPE is an integrated measure and thus comparable to total O<sub>3</sub> mixing ratio.

Numerous studies have determined OPE from observations to understand the efficacy of O<sub>3</sub> production and, with the support of models, probe the chemistry underlying changes in

O<sub>3</sub> production with emissions reductions. Reported observation-based OPE  $(\Delta O_3/\Delta NO_z)$  or  $\Delta O_x/\Delta NO_z$  values vary widely, from as low as 1 ppbv ppbv<sup>-1</sup> in urban areas to >100 ppbv ppbv<sup>-1</sup> in remote marine environments.<sup>39</sup> The general trend of increasing OPE with cleaner locations (i.e., urban to rural to remote marine) points to the nonlinear dependence of OPE on NO<sub>x</sub> and VOCs. It is well established that air masses with lower NO<sub>x</sub> mixing ratios or emissions tend to have higher observed OPE, such as in analyses of OPE in power plant plumes, 40 urban plumes, 32,41 and remote or rural areas. 42,43 Modeling studies support the trend of increasing OPE with decreasing NO<sub>x</sub> for both instantaneous and cumulative definitions of OPE. 17,33,44 Some models demonstrate this trend only above a certain NOx threshold, below which OPE has a positive correlation with  $NO_x$  (e.g.,  $NO_x$  threshold of  $\sim 0.2$ ppbv in Lin et al.,  $\sim$ 0.3 ppbv in Sillman and He, and  $\sim$ 1 ppbv in Mazzuca et al.),  $^{34,36,45}$  but this OPE turnover has not been observed experimentally. 46 Observation-based comparisons of OPE in low- versus high-VOC environments are rare in the literature.<sup>30</sup> However, modeling studies consistently demonstrate an increase in OPE with increasing VOCs or VOC reactivity (VOCR, the sum of VOC abundances multiplied by their OH reaction rate coefficients) over a broad range in  $\mathrm{NO}_{\scriptscriptstyle 33}$  33,34,44,47 and this understanding has been used to interpret the response of observation-based OPE to the counteracting impacts of NO<sub>x</sub> and VOC emission reductions. 48-50 Some studies have looked at the combined effect of emissions changes as the VOC/NO<sub>x</sub> ratio, finding an increase in OPE with increasing VOC/NO<sub>x</sub> in both observations and models. 41,51,52 Although OPE tends to be higher in NO<sub>x</sub>-sensitive environments and lower in NO<sub>x</sub>-saturated environments, an observation-based OPE alone does not allow definitive assignment of O<sub>3</sub> sensitivity regime (Section S1). Nonetheless, OPE provides valuable insight on how effectively NO<sub>x</sub> catalytically produces  $O_3$ , with implications for changes in total  $O_3$  production under different emission reduction scenarios.

The Atmospheric Emissions and Reactions Observed from Megacities to Marine Areas (AEROMMA) field campaign of June-August 2023 provided an unprecedented opportunity to determine OPE in the three largest US urban areas within a single O<sub>3</sub> season. The campaign utilized the NASA DC-8 aircraft, with a suite of in situ and remote sensing instruments, to address major science goals that included urban emissions and chemistry, remote marine emissions and chemistry, and validation of new geostationary satellite remote sensing capability.<sup>53</sup> The majority of the 148 total science flight hours during AEROMMA were spent on urban sampling patterns in New York City (NYC), Chicago, and Los Angeles (LA) during peak O<sub>3</sub> photochemistry months. In this work, we calculate OPE for these three cities from in situ observations of O<sub>3</sub> and reactive nitrogen species, and we examine the relationship between OPE and other measurements from the DC-8 platform. The results of this analysis help to define the current state of O<sub>3</sub> photochemistry in the three largest urban areas in the US, home to a combined 42 million people,<sup>54</sup> all of which are in nonattainment status for the current US National Ambient Air Quality Standard for  $O_3$ .55

#### 2. METHODS

**2.1.** In Situ Measurements for OPE Analysis. This analysis focuses on 11 of the 14 urban flights during AEROMMA. These include three of the four NYC flights (July 28, Aug. 9, Aug. 16; July 26 omitted due to lack of NO<sub>v</sub> data

for that flight), all of the Chicago flights (Aug. 1, 2, 8, 12, 15), and all of the LA flights (Aug. 23, 25, 26). The research flights in this analysis each included approximately 6 h of urban measurements, during which time the DC-8 made two to three "passes" (repeated raster patterns, e.g., Figure S1) within the boundary layer. Each pass began upwind of the metropolitan area and consisted of sequential downwind transects, ideally perpendicular to the prevailing wind direction. Typical transects were 20–50 km apart and flown at approximately level altitude (~550 magl). Table S1 summarizes the meteorological conditions for each of the analyzed flights. Transported smoke from the historic Canadian wildfires of 2023 influenced some of the NYC and Chicago flights but did not impact the results of this study, as addressed in Section 3.4

The DC-8 payload included two measurements of in situ  $O_x$  — the NOAA cavity ring-down spectrometer (CRDS)<sup>56,57</sup> measured  $O_x$  directly, while the sum of the NOAA fast-response chemiluminescence (CL)<sup>58</sup>  $O_3$  and the NOAA laser-induced fluorescence (LIF)<sup>59,60</sup>  $NO_2$  provided an additional  $O_x$  measurement (CL + LIF  $O_x$ ) — and the difference of LIF  $NO_y$ ,  $NO_2$ , and NO enabled calculation of in situ  $NO_z$  (instrument details in Section S2). Together, these measurements enabled determination of observed OPE. Many other measurements from the DC-8 payload, listed in Table S2, also contributed to the analysis.

**2.2. OPE Calculation Method.** An accurate OPE calculation requires that the slope of the regression  $(\Delta O_x/\Delta NO_z)$  represents the urban plume enhancement above constant background mixing ratios, rather than the effects of mixing between air masses with different emissions, meteorology, and photochemistry. The DC-8 was often unable to traverse the entirety of the plume during AEROMMA due to flight pattern restrictions, so we were unable to compare plume-edge mixing ratios of urban tracers (e.g., CO) as a method for transect filtering, as done in previous analyses. Instead, we first employed several methods to refine the bounds of each transect, and then we tested the sensitivity of the city mean OPEs to the application of different transect-elimination filters.

Across a level transect, where pressure and temperature are expected to remain constant, abrupt changes in potential temperature may indicate a difference in vertical mixing. Steps in relative humidity, especially for transects near the shore of a lake or ocean, may similarly indicate a mixing boundary between two airmasses. We used changes in potential temperature, relative humidity and/or altitude to trim or split transects. The regression of NO<sub>v</sub> versus CO across the transect (slope =  $\Delta NO_{\nu}/\Delta CO$ ) provided an additional refinement technique, where NO<sub>v</sub> serves as a proxy for emitted NO<sub>x</sub>.<sup>29</sup> A strong positive  $\Delta NO_v/\Delta CO$  correlation indicates a constant emission ratio, typically dominated by motor vehicle emissions, in the sampled air mass. Transect  $\Delta NO_{\nu}/\Delta CO$  regressions showing two discrete populations or distinct curvature, indicative of the mixing of air masses with different emission sources, were either trimmed or split into separate transects before calculating OPE (e.g., Figure S1); no transects were eliminated based on  $\Delta NO_{\nu}$  $\Delta$ CO correlation. There were 196 total transects in the analysis after applying these refinement methods.

The OPE was calculated from a linear regression of the  $O_x$  and  $NO_z$  measurements for each individual transect across the urban plume, where the slope is the OPE  $(\Delta O_x/\Delta NO_z)$  and the *y*-intercept is the theoretical background  $O_x$  mixing ratio when  $NO_z$  equals zero (Figure S2). The results presented in the main text, and in the SI unless explicitly noted, use directly measured

CRDS O<sub>x</sub> for OPE calculation and subsequent analysis. A second version of the analysis was conducted in parallel using summed CL + LIF O<sub>x</sub>, resulting in OPEs on average 25% higher than those calculated with CRDS  $O_x$  (within the city-wide mean OPE uncertainty) and demonstrating the same trends (Tables S3 and S4 and Figure S3). For each transect, an ordinary leastsquares (OLS) linear regression was first used to assess the correlation strength via the coefficient of determination  $(R^2)$ , and then the transect data were evaluated with a weighted orthogonal distance regression (ODR) linear fit 51,62,63 to obtain the final transect OPE values. Two filters were applied to eliminate transects that may not represent the chemistry in the plume, resulting in a final total of 153 transects in the analysis (additional details in Sections S3 and S4 and Tables S3 and S4). All OPEs reported in this analysis are upper limits due to the potential for dry deposition of HNO3 that may systematically reduce observed NO<sub>z</sub> and thus enhance the apparent OPE. <sup>29,33,61</sup> We found that correcting the observed transect NO<sub>2</sub> for HNO<sub>3</sub> dry deposition lowered the city mean OPE by 3-30%, depending on the literature dry deposition velocity, estimated boundary layer height, and estimated transport time used in the calculation, and the corrections had no impact on the reported trends (Figure S4 and Section S5).

2.3. Zero-Dimensional Photochemical Box Modeling **of OPE.** We probed the chemistry driving observed OPE values with a simple photochemical box model using the Framework for 0-Dimensional Atmospheric Modeling (F0AM)<sup>64</sup> with the full Master Chemical Mechanism (MCMv3.3.1) as the nearexplicit gas-phase mechanism. 65 The intent of the model was not to comprehensively model an urban plume, but rather to understand the dependence of OPE on NO<sub>x</sub> and VOCs. First, we modeled the observations from a single transect from the Aug. 2 Chicago flight, which we will henceforth call the "target transect." We chose to model this transect for several reasons: its location over Lake Michigan on a day with south-southwesterly winds allows for the assumption that emissions predominantly come from land-based urban sources at time zero (Figure S5); the target transect observed OPE  $(8 + 2/-3 \text{ ppbv ppbv}^{-1})$  falls within the uncertainty of the mean OPE for each of the three cities, and the high mean  $(\pm 2\sigma)$  O<sub>3</sub> measured across the transect  $(81 \pm 2 \text{ ppbv})$  is representative of a high  $O_3$  day in the Chicago metropolitan area. We define a section of the flight path west of the target transect, outside of the urban plume, as the "background transect." The model setup and inputs, described extensively in Section S6, are summarized here.

The model is a Lagrangian framework and is initialized with mixing ratios of VOCs and  $NO_x$  that are representative of emissions from biogenic and anthropogenic sources. The model assumes that the evolution of a chemical species is determined by reaction and dilution with background air (eq 2),

$$\frac{\mathrm{d}C_i}{\mathrm{d}t} = \sum r_i(t) - k_{\mathrm{dil}}(C_i - C_{\mathrm{b},i}) \tag{2}$$

where  $C_i$  is the concentration of species i,  $r_i(t)$  represents the time-dependent reaction rate for species i (sum of gas-phase chemical production and loss terms), and dilution is parametrized by a first-order rate coefficient  $(k_{\rm dil})$  and the background (*i.e.*, out-of-plume) species concentration  $(C_{\rm b,i})$ . For HNO<sub>3</sub>, we also include a first-order dry deposition loss term. The model run length of 5 h represents the approximate transport time between the urban center and the target transect as determined from a HYSPLIT back-trajectory analysis. <sup>66</sup> Background concentrations for all species were set as the mean

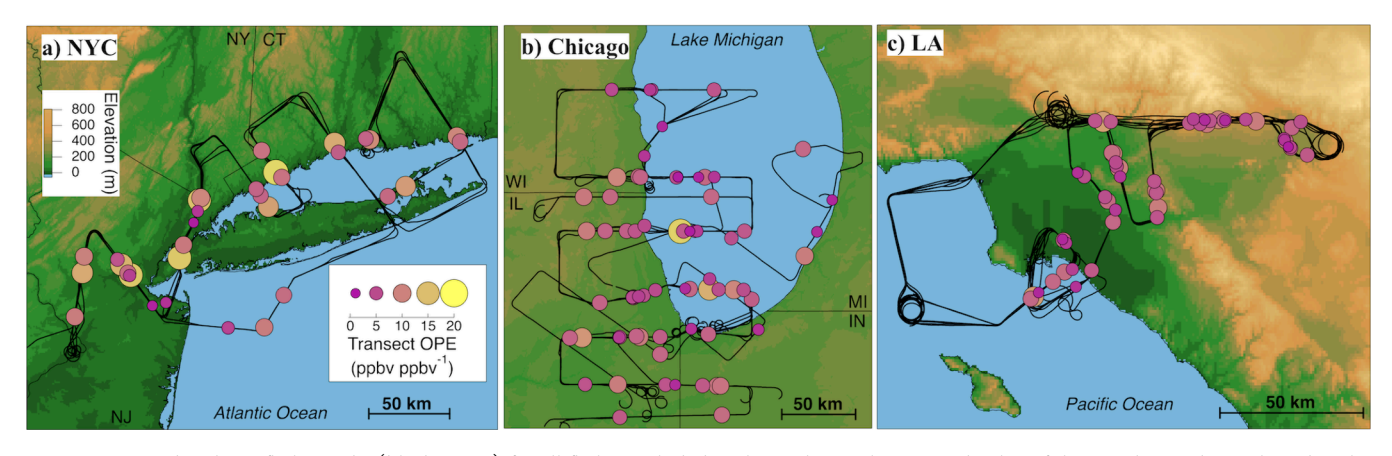


**Figure 1.** Boundary layer flight tracks (black traces) for all flights included in the analysis. The size and color of the circular markers, plotted at the center of each transect, indicate the magnitude of the observed OPE at that transect. The legends in panel (a) apply to all three panels.

observed mixing ratios across the background transect. The initial concentrations ( $C_{i,t=0}$ ) of primary species in the model, such as  $NO_x$  and isoprene, were estimated using an iterative scheme (see below), while the initial concentrations of secondary species in the model, such as  $O_3$  and PAN, were set equivalent to the background concentration for that species. The model was constrained with measured temperature, pressure, water vapor, and  $NO_2$  photolysis rate ( $jNO_2$ ) across the target transect.

The "base model" was determined by iterating initial concentrations of primary species and tuning  $k_{dil}$  until model output  $O_3$ ,  $NO_2$ ,  $NO_3$ , and VOCR agreed within  $\pm 2\sigma$  of the observed target transect mean, and observed and modeled OPE agreed within the observed OPE uncertainty (Section S6). We subsequently used the base model for OPE sensitivity tests (see Section S7 for details). Briefly, a range of initial NO<sub>x</sub> values (0.1) to 100 ppbv) and initial primary VOC scaling factors (0.1 to 15) were applied to the model. Each sensitivity test consisted of a single model run in which the base model was perturbed with a unique combination of initial NO<sub>x</sub> and primary VOC scaling, and the final model OPE, time-averaged VOCR, and final species mixing ratios were recorded. The modeled OPE was calculated as the enhancement ratio of O<sub>x</sub> to NO<sub>x</sub> (eq 1), where the enhancement as represented in the model is the difference between the final modeled mixing ratio and background mixing ratio of  $O_x$  and  $NO_z$ , respectively.

# 3. RESULTS AND DISCUSSION

The arithmetic mean  $(\pm 1\sigma)$  OPE during AEROMMA in NYC was  $9 \pm 4$  ppbv ppbv<sup>-1</sup>, while the mean OPE for both Chicago and LA was  $6 \pm 3$  ppbv ppbv<sup>-1</sup>. Table S7 provides the mean OPE for each individual flight along with other city-wide statistics. Ozone production efficiency depends on a variety of factors within urban areas. In the following, we investigate the dependence of OPE on: the spatial distribution of emissions and their interaction with local meteorology, the chemical plume age and local time of day, concentrations of NO<sub>x</sub>, concentrations of VOCs and VOCR, and the ratio of VOC to NO<sub>x</sub>.

**3.1. Spatial Dependence of OPE.** Since OPE is an integrated measure of photochemistry in an air parcel that has a different dependence on  $NO_x$  and VOCs than total  $O_3$  mixing ratio or production rate, its spatial distribution may differ from that of maximum  $O_3$  mixing ratios. We examine this relationship in each of the three cities in Figure 1, where transect OPEs are overlain on the boundary layer flight tracks in that city.

Coastal meteorology, and its association with O<sub>3</sub> exceedances, is a long-standing area of research. 67-69 In addition to elevated O<sub>3</sub> in NYC itself, the downwind, densely populated regions of Long Island and southern Connecticut regularly experience high surface O<sub>3</sub> due to coastal circulation patterns. <sup>70</sup> The NYC urban plume frequently transports from the southwest with the prevailing morning winds over Long Island Sound, where pollutants may be concentrated within the shallow marine boundary layer before experiencing onshore transport from sea breeze meteorology in the afternoons or evenings.<sup>69,71</sup> The spatial distribution of transect OPEs in this work does not align strongly with the usual location of high O<sub>3</sub> mixing ratios in the NYC metro area (Figure 1a and Figure S7a). Because meteorology (Table S1) and maximum O3 concentrations were variable during the NYC flights, the AEROMMA observation-based OPEs may not represent a typical NYC metro area O3 exceedance day.

In Chicago, the highest O<sub>3</sub> values in the region consistently occur on the shore of Lake Michigan. 72 Several modeling studies point to lake-land breeze circulation as a driver for this spatial pattern in O3 exceedances. High O3 production rates tend to occur over the surface of Lake Michigan, 73,74 and the mixed layer above the lake — which frequently remains shallow and stable throughout the day and demonstrates suppressed vertical mixing — enables persistent high O<sub>3</sub> over the water despite a lack of fresh emissions. The lake breeze, predominately from the southeast, then transports high O3 onto the western shore of Lake Michigan. 67,76 The distribution of Chicago transect OPEs in the present analysis do not show strong spatial trends, regardless of wind direction or maximum observed O3 on the flight day (Figure 1b and Figure S7b,d). The AEROMMA data thus suggest that high lakeshore O3 results from the unique meteorology of Lake Michigan rather than a shift in chemistry at the shoreline.

The topography and meteorology of the LA Basin has a well-understood influence on the location of maximum O<sub>3</sub> mixing ratio. With a strong westerly sea breeze that transports polluted air inland, monitoring sites in the eastern part of the LA Basin have historically experienced the highest and most persistent O<sub>3</sub>. The shift in the LA Basin O<sub>3</sub> sensitivity regime over the past decade, from more to less NO<sub>3</sub>-saturated, impacts the location of the highest O<sub>3</sub> mixing ratios. The present study, however, transect OPEs show no spatial dependence across the region (Figure 1c and Figure S7c), consistent with OPE as a measure that is independent of O<sub>3</sub> mixing ratio itself.

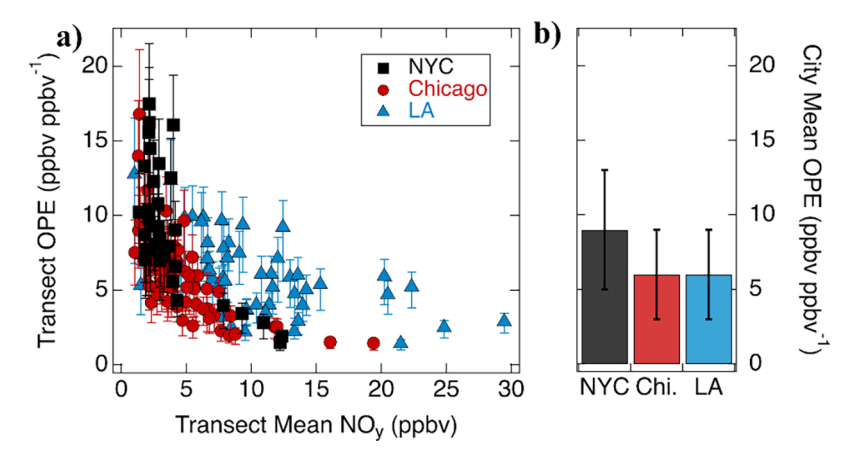
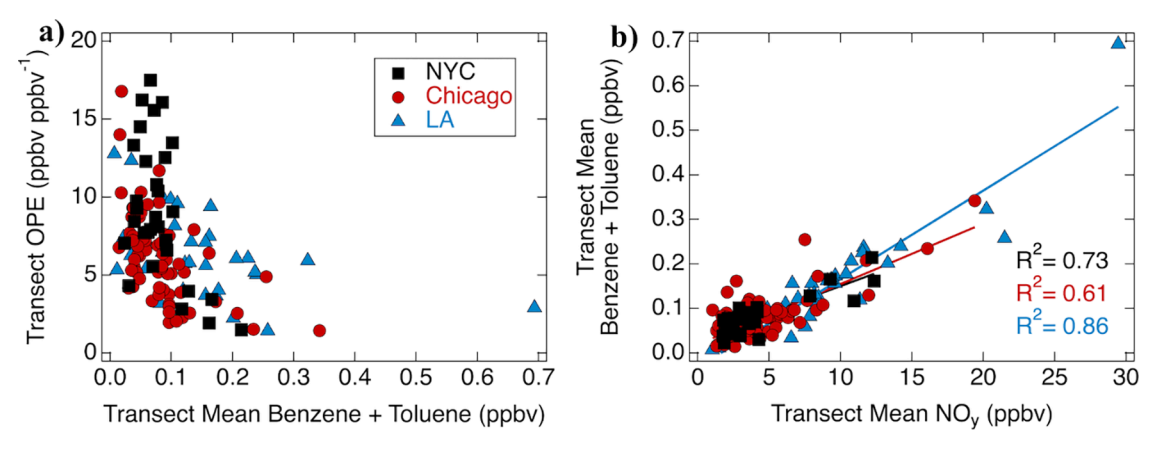


Figure 2. (a) Ozone production efficiency at each transect plotted against mean NO<sub>y</sub>. The asymmetric OPE error bars incorporate weighted ODR fit error, systematic measurement uncertainty, and uncertainty due to NO<sub>z</sub> loss (see Section S3 and S5 for details). (b) Mean OPE for each city, where error bars represent  $\pm 1\sigma$ .



**Figure 3.** (a) Ozone production efficiency at each transect plotted against mean benzene + toluene as a tracer for fossil fuel VOCs. (b) Transect mean benzene + toluene plotted against mean  $NO_y$ , with OLS linear fit (solid lines)  $R^2$  values appearing in each city's corresponding color. The legends in panel (a) apply to both panels. See Figure S11 for equivalent plots with VCPs, biogenic VOCs, and VOCR.

**3.2. Temporal Dependence of OPE.** We assessed two temporal variables for their potential impacts on OPE: chemical plume age and the time of day. Observations of  $NO_x$  and  $NO_y$  across each transect enable an estimation of the chemical age of the plume at the time of measurement (t), where  $\tau$  (= 1/k') is the effective  $NO_x$  lifetime (eq 3). Although  $\tau$  is unknown for these transects, if  $\tau$  is approximately constant then the natural log of the  $\Delta NO_x/\Delta NO_y$  enhancement ratio yields a value that is proportional to chemical plume age (eq 4); if  $NO_x$  emissions are continuous rather than from a discrete source, this equation provides an average measure of chemical plume age.

$$\frac{[\text{NO}_x]}{[\text{NO}_y]} \approx \frac{[\text{NO}_x]_t}{[\text{NO}_x]_0} = \exp(-\frac{t}{\tau})$$
(3)

$$t \propto \ln \frac{[NO_x]}{[NO_y]}$$
 (4)

Within a single air parcel, modeled instantaneous OPE is expected to increase with plume age due to the reduction in  $NO_x$  over time.<sup>32</sup> Studies of observation-based OPEs in a single plume (*i.e.*, the integrated sum of instantaneous OPEs) have also found an increase in OPE with plume age.<sup>33,40,83</sup> In our analysis, however, the value of the calculated OPEs do not have a strong dependence on this measure of chemical plume age (Figure S8).

There is no positive correlation between OPE and the locally observed  $jNO_2$  (Figure S9), although there is a weak positive correlation ( $R^2 = 0.43$ ) between OPE and local time in LA only (Figure S10). Increased photolysis rates, for which  $jNO_2$  is a proxy, increase the total primary radical source and thus the rate of instantaneous  $O_3$  production for a given amount of  $NO_x$ . The lack of dependence of OPE on photolysis rates demonstrates that OPE is an integrated rather than instantaneous quantity.

**3.3. OPE Dependence on NO\_x.** The transect OPEs determined from aircraft observations during AEROMMA display a strong inverse, nonlinear dependence on the mean transect NO, in all three cities (Figure 2a). The use of NO, on the x-axis serves as a proxy for  $NO_x$  in the plume at the time of emission.<sup>29</sup> The OPEs for NYC and Chicago fall on a similar curve, while the OPEs for LA have a somewhat different dependence, as we explore further in Sections 3.4-3.6. This demonstrates that cities with a similar mean OPE (Figure 2b) may not necessarily have a similar OPE dependence on emitted  $NO_x$  (i.e.,  $NO_v$ ). The inverse relationship between observationbased OPE and NO<sub>x</sub> during AEROMMA is similar to that in the literature where both OPE and NO<sub>x</sub> observations are reported, such as the dependence of aircraft-based OPEs on NO<sub>x</sub> in Phoenix, Arizona (May 1998)<sup>32</sup> and the dependence of groundbased summer OPE on NOz in the southeastern US (1996-2014). 84 We compare the AEROMMA observation-based OPEs

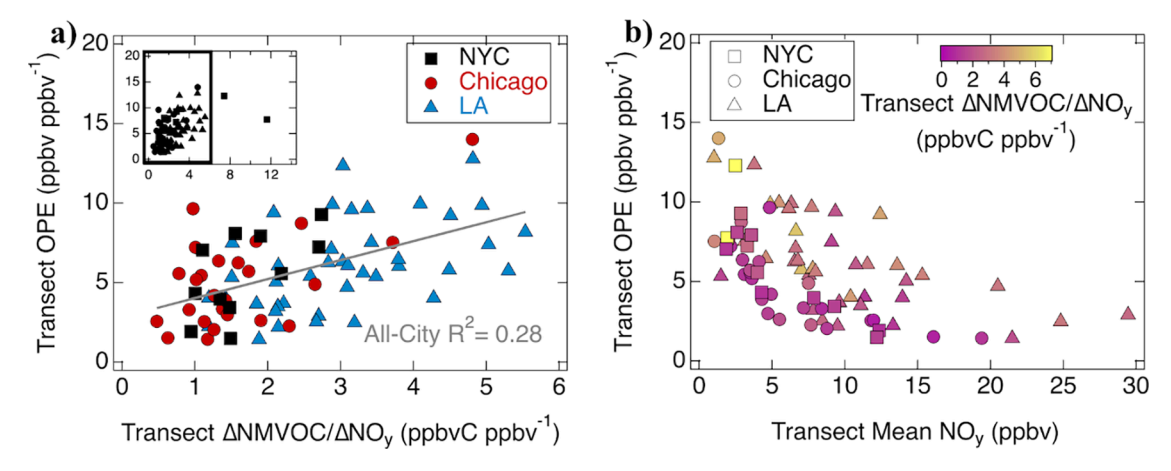


Figure 4. (a) Ozone production efficiency at each transect plotted against the  $\Delta \text{NMVOC}/\Delta \text{NO}_y$  enhancement ratio. Transects with  $\Delta \text{NMVOC}/\Delta \text{NO}_y$  OLS fit  $R^2 < 0.5$  are excluded. The inset figure shows the full *x*-axis, while the main figure excludes the two NYC outlier points. Ordinary least-squares fit (solid line)  $R^2$  value for all cities together, excluding the two outlier points, is 0.28. (b) Transect OPE plotted against mean NO<sub>y</sub> and colored by  $\Delta \text{NMVOC}/\Delta \text{NO}_y$ .

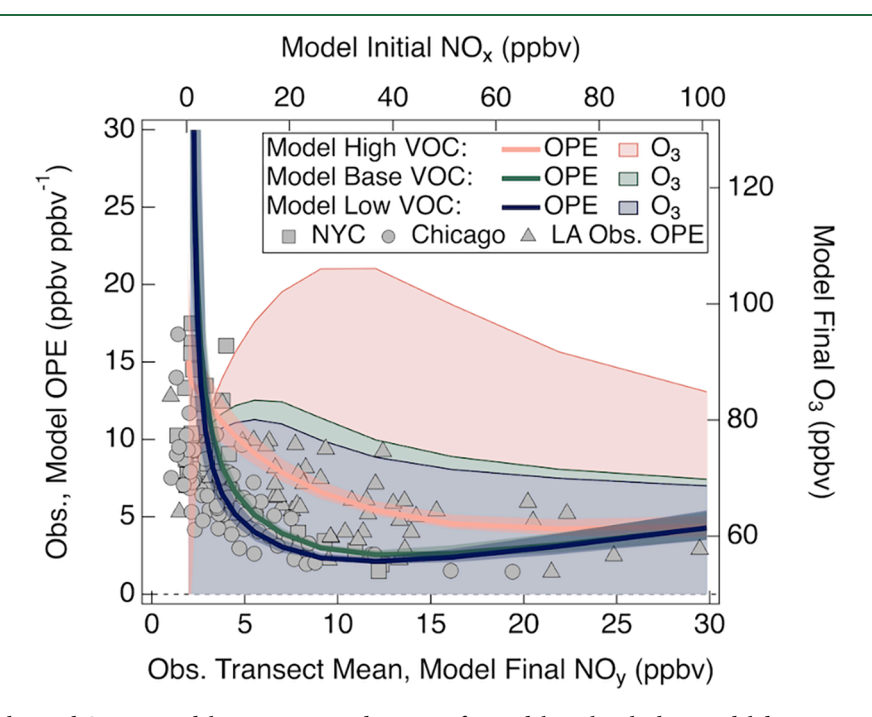


Figure 5. Comparison of observed OPE to model output to provide context for model results; the box model does not necessarily represent the true position of the observed transects on an OPE or total  $O_3$  curve. Observed OPE at each transect is plotted against mean observed NO $_y$  (gray markers). Solid lines represent model OPE (translucent error shading represents model sensitivity to transport time, photolysis rate scaling, and background mixing ratios) and solid shading represents model final  $O_3$  for low  $(0.1\times)$ , base  $(1\times)$ , and high  $(10\times)$  initial primary VOC scaling. Corresponding mean time-averaged model VOCR for low, base, and high VOC scaling is 1.8, 2.7, and 13 s<sup>-1</sup>, respectively.

to historical OPE values and emissions trends in NYC and LA in Section 3.6.

**3.4. OPE Dependence on VOCs.** To investigate possible OPE correlations with VOCs from different emissions sources, we identified three tracer VOCs (or groups of VOCs) that are relatively long-lived and come predominantly from a single emission sector: the sum of benzene and toluene as a tracer for fossil fuel emissions; <sup>85,86</sup> decamethylcyclopentasiloxane (D5 siloxane) as a tracer for VCP emissions; <sup>87</sup> and the sum of isoprene and two of its major oxidation products, methyl vinyl ketone (MVK) and methacrolein (MACR), as a tracer for biogenic emissions (Table S8). Measurements of total OH reactivity and speciated VOCs during AEROMMA indicate that these three sources of VOCs make up the majority of identifiable

urban VOCR during the campaign. <sup>88</sup> We also calculated VOCR from observed OH reactivity (Table S2 and Section S8), however VOCR provides limited insights because it is an instantaneous rather than integrated metric. In Figure 3a, transect OPEs demonstrate a nonlinear, inverse correlation with fossil fuel tracer VOCs in all three cities that mirrors the nonlinear correlation between OPE and NO $_y$  (Figure 2a). There is a strong positive correlation between fossil fuel VOCs and transect mean NO $_y$  (Figure 3b; NYC  $R^2$  = 0.73, Chicago  $R^2$  = 0.61; LA  $R^2$  = 0.86). If the dependence of OPE on NO $_x$  is stronger than the relationship between OPE and VOCs, then the apparent dependence of OPE on fossil fuel VOCs in Figure 3a is a result of colocated NO $_x$  and VOC sources. We test this hypothesis using a photochemical box model in Section 3.5.

Figure S11a-f present equivalent figures for VCPs, biogenic VOCs, and VOCR. The correlation of OPE with VCPs (Figure S11a) is similar to Figure 3a, and there is also a strong positive correlation between VCPs and NO<sub> $\nu$ </sub> (Figure S11b; NYC  $R^2$  = 0.90; Chicago  $R^2 = 0.86$ ; LA  $R^2 = 0.73$ ). In contrast, there is little to no correlation between biogenic VOCs and OPE or NO, (Figure S11c,d;  $R^2$  < 0.30 for all cities). The correlation between OPE and VOCR is very weak for all cities ( $R^2 < 0.20$ ; Figure S11e), while the correlation between VOCR and NO, (Figure S11f) is strong in LA ( $R^2 = 0.68$ ) and weak in Chicago  $(R^2=0.36)$ . The lack of correlation between VOCR and NO<sub> $\nu$ </sub> in NYC may be due to the influence of biogenic VOCs, which do not correlate with NO, in NYC (Figure S11d). Additionally, there is no strong dependence of OPE on acetonitrile (ACN), a biomass burning tracer VOC, allowing us to conclude that transported wildfire smoke during summer 2023 did not significantly impact our results (Section S9 and Figure S12).

From the OPE modeling literature discussed in Section 1, we expect an increase in OPE with increasing VOCs or VOCR, 33,34,44,47 but this dependence is difficult to distinguish in the simple correlations shown thus far. We next assess the dependence of OPE on the nonmethane VOC (NMVOC) to NO<sub>v</sub> enhancement ratio as an estimate of the VOC/NO<sub>x</sub> ratio. We calculate  $\Delta NMVOC/\Delta NO_y$  as the weighted ODR slope of the carbon-weighted sum of calibrated, in situ VOCs (Table S8) against NO, across the transect, omitting transects with OLS fit  $R^2$  < 0.5 from the subsequent analysis. Because this  $\Delta$ NMVOC/  $\Delta NO_{\nu}$  calculation does not include integrated whole-air sampler VOC canister samples, the magnitude is an underestimate due to the omission of alkanes and small alkenes, but the trend with OPE is informative. There is a positive correlation between transect OPE and  $\Delta$ NMVOC/ $\Delta$ NO $_{\nu}$  in all three cities (Figure 4a; NYC  $R^2 = 0.38$  with two outlier points excluded; Chicago  $R^2$ = 0.37; LA  $R^2$  = 0.25), as has been observed in the literature. 41,51,52 However, since both increasing VOCs and decreasing emitted NO<sub>x</sub> lead to increased  $\Delta$ NMVOC/ $\Delta$ NO<sub>y</sub> and are also expected to increase OPE, this correlation alone does not provide further information about the dependence of OPE on VOCs compared to NO<sub>x</sub>. Figure 4b effectively demonstrates that increased VOCs correlate with increased OPE, where  $\Delta NMVOC/\Delta NO_{\nu}$  helps to explain the variation in OPE for similar values of transect mean NO,

**3.5.** Modeled OPE Dependence on  $NO_x$  and VOCs. The zero-dimensional photochemical box model for the Aug. 2 Chicago target transect was iterated to achieve agreement (within  $\pm 2\sigma$  of the target transect mean, or within OPE uncertainty) between modeled and observed OPE (modeled =  $8.2 \pm 0.6$  ppbv ppbv<sup>-1</sup>; observed = 8 + 2/-3 ppbv ppbv<sup>-1</sup>),  $O_3$ ,  $NO_z$ ,  $NO_x$ , and VOC reactivity (Figure S13). The model also agreed with observations of the top four contributors to model VOC reactivity (Figure S14): formaldehyde (modeled as a secondary species), acetaldehyde, methanol, isoprene (modeled as primary species, *i.e.*, constrained). This representation of the target transect was then used as the base model upon which to test the response of OPE to perturbations in initial  $NO_x$  and primary VOCs.

Figure 5 presents a comparison of the OPE observations at each transect to the model OPE and model final  $O_3$ . The model curves represent a subset of the six initial primary VOC scaling factors tested: 0.1× scaling as "low VOC" (mean of time-averaged model VOCRs for each model run at this VOC scaling is 1.8 s<sup>-1</sup>), 1× scaling as "base VOC" (mean VOCR is 2.7 s<sup>-1</sup>), and 10× scaling as "high VOC" (mean VOCR is 13 s<sup>-1</sup>). To

facilitate comparison between the observations and the model, the model OPE and O<sub>3</sub> curves are plotted against final model NO<sub>v</sub> on the bottom axis, with the corresponding model initial  $NO_x$  on the top axis. The intent of the comparison in Figure 5 is to provide an observational context for the modeled dependence of OPE on NO<sub>x</sub> and VOCs; perturbations of a single base model cannot accurately represent all of the observed transects with respect to their position on an OPE or total O<sub>3</sub> versus NO<sub>r</sub> curve. The model-observation comparisons are therefore qualitative rather than quantitative. For the majority of the observed NO<sub>v</sub> values, both modeled and observed OPE increase with decreasing initial  $NO_x$  (final  $NO_y$ ). Trends in model final O<sub>3</sub>, O<sub>r</sub>, NO<sub>2</sub>, OH, and HO<sub>2</sub> as a function of initial NO<sub>x</sub> and primary VOC scaling factors (Figure S15) help to explain the chemistry driving the model OPE, as discussed further in Section S10. The agreement of the high VOC model OPE curve with many of the LA observations suggests that high VOCs (high VOCR) in LA could explain the elevated values of observed OPE despite corresponding high values of measured NO<sub>w</sub> as Figure 4b also supports. Robust comparisons between observed and modeled OPE break down below the value of the observed background NO, mixing ratio, 2.3 ppbv (~1.5 ppbv model initial NO<sub>x</sub>), because the background mixing ratios in the model remain fixed regardless of the initial model NO<sub>x</sub> perturbation. The model OPE error shading captures some of uncertainty induced by this effect (Section S7).

3.6. Observed and Modeled OPE in the Context of **Historical Measurements.** The results of the observations and model help us to understand historical trends in OPE with changing emissions in NYC and LA. To our knowledge, there are no historical, observation-based OPEs reported in Chicago. From 1996 to 2023, inventory NO<sub>x</sub> emissions (expressed as mass of NO<sub>2</sub>) in New York state decreased from ~8 to 2 Mtons yr<sup>-1</sup>. 89 Over the same period, the mean OPE in NYC increased from 2–4 ppbv ppbv<sup>-1</sup> in 1996 (OPE defined as  $\Delta O_3/\Delta NO_z$ ; the equivalent  $\Delta O_x/\Delta NO_z$  value may be slightly higher), 90 to  $6-8 \text{ ppbv ppbv}^{-1} \text{ in } 2016,^{46} \text{ to } 9 \pm 4 \text{ ppbv ppbv}^{-1} \text{ in } 2023$ during AEROMMA (Figure S16). In contrast, over the period 1973 to 2010 in LA, Pollack et al. (2013) found no discernible trend in OPEs determined from field campaign data despite statistically significant decreases in both NO<sub>x</sub> and VOCs, likely due in part to the counteracting effects of these decreases on OPE. 51 The two most recent airborne field campaigns (ARCTAS-CARB in 2008, CalNex in 2010) in the analysis both measured OPEs of ~6 ppbv ppbv<sup>-1</sup>, and the mean observed LA OPE in 2023 during AEROMMA was also  $6 (\pm 3)$ ppbv ppbv $^{-1}$ , although NO<sub>x</sub> emissions decreased over the intervening period. <sup>7,91</sup> In the observation-based component of our analysis, the dependence of individual transect OPEs on emitted NO<sub>x</sub> during AEROMMA align with these historical trends; the individual transect OPEs in NYC have a stronger dependence on (change more steeply with) transect NO, than those in LA.

Our model results suggest an explanation for these different trends in OPE despite similar reductions in  $NO_x$  and VOCs across the US. In Figure S17, we consider the lower and upper quartiles of the mean  $NO_y$  values for all OPE transects to roughly represent  $NO_x$ -sensitive and  $NO_x$ -saturated conditions, respectively. The position of the  $NO_y$  quartiles with respect to the base model total  $O_3$  curve supports this approximation. Observed OPEs for all three cities have larger variability ( $\sigma = 3$  ppbv ppbv<sup>-1</sup>) under  $NO_x$ -sensitive conditions compared to  $NO_x$ -saturated conditions ( $\sigma = 2$  ppbv ppbv<sup>-1</sup>). This variability is

consistent with model OPE predictions, which vary strongly with  $NO_x$  in the  $NO_x$ -sensitive regime but vary little with  $NO_x$  in the  $NO_x$ -sensitive regime. Therefore, we expect OPE under more  $NO_x$ -sensitive conditions to have a stronger response to decreases in  $NO_x$  emissions. We also compare the distribution of OPE for individual cities under different  $O_3$  sensitivity regimes (Table S9). Across all three cities,  $NO_x$ -sensitive conditions correspond to larger and more variable OPEs when compared to  $NO_x$ -saturated conditions. The OPE distribution in LA presents an interesting example of the nuance within a city-wide mean OPE. LA has a higher  $NO_x$ -saturated mean OPE than NYC and Chicago, likely due to higher VOCR (Figure 5), yet the overall mean OPE in LA is lower than that in NYC because of overall higher  $NO_x$  in LA.

# 4. IMPLICATIONS FOR NO<sub>X</sub>-VOC O<sub>3</sub> MITIGATION STRATEGIES

We analyzed the efficiency of summertime urban  $O_3$  production across the largest US urban areas during July–August 2023. Mean aircraft-based OPEs were  $9\pm4$ ,  $6\pm3$ , and  $6\pm3$  ppbv ppbv<sup>-1</sup> in NYC, Chicago, and LA, respectively, marking an increase in OPE in NYC but not in LA when compared to available historical data. The observations show a distinct increase in OPE with decreasing  $NO_y$ , and an increase in OPE with increasing  $\Delta NMVOC/\Delta NO_y$ , in all three cities. The observations exhibit no strong spatial or temporal relationship with OPE. A zero-dimensional photochemical box model describes the observed OPE, providing qualitative insight into the chemistry driving the nonlinear dependence of OPE on  $NO_x$  and VOCs and the distinction between OPE and total  $O_3$  production. This analysis emphasizes several important attributes of urban OPE:

- 1. NO<sub>x</sub> produces O<sub>3</sub> most efficiently at the lowest NO<sub>x</sub> values. Therefore, at low NO<sub>x</sub>, OPE continues to increase even as total O<sub>3</sub> production decreases with decreasing NO<sub>x</sub>. For example, at ~5 ppbv initial NO<sub>x</sub> and model base VOC scaling (Figure 5), a 20% reduction in emitted NO<sub>x</sub> increases OPE by 9% but nonetheless reduces O<sub>3</sub> by 1%. Although an increasing OPE means that each individual emitted NO<sub>x</sub> molecule produces more O<sub>3</sub>, reducing NO<sub>x</sub> emissions (when NO<sub>x</sub> is low) still effectively reduces total O<sub>3</sub> production.
- 2. At most urban levels of NO<sub>x</sub> decreases in VOCs or VOCR will decrease OPE. Concomitant reductions in NO<sub>x</sub> and VOCs may have a counteracting impact on OPE, especially when the range in possible OPE values is relatively small (when NO<sub>x</sub> is high). The opposing dependencies of OPE on NO<sub>x</sub> and VOCs both drive the increase in OPE with an increasing VOC/NO<sub>x</sub> ratio.
- 3. Ozone production efficiency increases most steeply with decreasing NO<sub>x</sub> at low NO<sub>x</sub> values, whereas OPE changes relatively slowly with decreasing NO<sub>x</sub> at high NO<sub>x</sub> values. This means that observed OPEs in NO<sub>x</sub>-sensitive photochemical regimes likely have higher variability, and a larger response to NO<sub>x</sub> emissions reductions, compared to more NO<sub>x</sub>-saturated regimes.
- 4. Without comprehensive and location-specific modeling, a single OPE does not indicate the photochemical regime that dictates O<sub>3</sub> production; similar OPE spatially or temporally does not necessarily mean that the O<sub>3</sub> production regime is the same. Instead, an observation-based OPE analysis, such as that presented here,

elucidates the efficiency of  $NO_x$  as an  $O_3$  formation catalyst and how this efficiency may change with emissions reductions. This analysis illustrates the value of combined measurements of  $O_x$  and  $NO_z$  component species  $(O_3, NO_2, NO_x, NO_x)$  and  $NO_y)$  to facilitate the calculation of OPE. Consideration of observation-based OPE alongside total  $O_3$  production or  $O_3$  production rates will enhance the understanding of urban  $O_3$  photochemistry in the context of changing  $NO_x$  and VOC emissions.

# ASSOCIATED CONTENT

#### **Data Availability Statement**

The data underlying this study are publicly available on the AEROMMA data archive:https://csl.noaa.gov/projects/aeromma/data.html.

# Supporting Information

The Supporting Information is available free of charge at https://pubs.acs.org/doi/10.1021/acs.est.5c02073.

Text, figures, and tables containing additional descriptions of instrumentation, analysis methods, box model setup, and results (PDF)

# AUTHOR INFORMATION

#### **Corresponding Author**

Steven S. Brown — NOAA Chemical Sciences Laboratory,
Boulder, Colorado 80305, United States; Department of
Chemistry, University of Colorado Boulder, Boulder, Colorado
80309, United States; orcid.org/0000-0001-7477-9078;
Email: steven.s.brown@noaa.gov

#### **Authors**

Wyndom S. Chace — Cooperative Institute for Research in Environmental Sciences and Department of Chemistry, University of Colorado Boulder, Boulder, Colorado 80309, United States; NOAA Chemical Sciences Laboratory, Boulder, Colorado 80305, United States; orcid.org/0009-0009-1951-2050

Caroline Womack — NOAA Chemical Sciences Laboratory, Boulder, Colorado 80305, United States; orcid.org/0000-0002-7101-9054

Katherine Ball – Division of Chemistry and Chemical Engineering, California Institute of Technology, Pasadena, California 91125, United States

Kelvin H. Bates — Cooperative Institute for Research in Environmental Sciences, University of Colorado Boulder, Boulder, Colorado 80309, United States; NOAA Chemical Sciences Laboratory, Boulder, Colorado 80305, United States; Present Address: Department of Mechanical Engineering, University of Colorado Boulder, Boulder, Colorado 80309, United States (K.H.B.)

Birger Bohn − Institute of Climate and Energy Systems, ICE-3: Troposphere, Forschungszentrum Jülich, Jülich 52428, Germany; orcid.org/0000-0003-4177-3934

Matthew Coggon − NOAA Chemical Sciences Laboratory, Boulder, Colorado 80305, United States; ocid.org/0000-0002-5763-1925

John D. Crounse — Division of Geological and Planetary Sciences, California Institute of Technology, Pasadena, California 91125, United States; orcid.org/0000-0001-5443-729X

- Hendrik Fuchs Institute of Climate and Energy Systems, ICE-3: Troposphere, Forschungszentrum Jülich, Jülich 52428, Germany; Department of Physics, University of Cologne, Cologne 50937, Germany; orcid.org/0000-0003-1263-0061
- Jessica Gilman − NOAA Chemical Sciences Laboratory, Boulder, Colorado 80305, United States; ocid.org/0000-0002-7899-9948
- Georgios I. Gkatzelis Institute of Climate and Energy Systems, ICE-3: Troposphere, Forschungszentrum Jülich, Jülich 52428, Germany; orcid.org/0000-0002-4608-3695
- Christopher M. Jernigan Cooperative Institute for Research in Environmental Sciences, University of Colorado Boulder, Boulder, Colorado 80309, United States; NOAA Chemical Sciences Laboratory, Boulder, Colorado 80305, United States; Present Address: Office of Research and Development, U.S. Environmental Protection Agency, Research Triangle Park, NC 27711, United States (C.M.J.)
- Gordon A. Novak NOAA Chemical Sciences Laboratory, Boulder, Colorado 80305, United States; ⊚ orcid.org/0000-0003-4009-039X
- Anna Novelli Institute of Climate and Energy Systems, ICE-3: Troposphere, Forschungszentrum Jülich, Jülich 52428, Germany; orcid.org/0000-0003-2077-7573
- Jeff Peischl Cooperative Institute for Research in Environmental Sciences, University of Colorado Boulder, Boulder, Colorado 80309, United States; NOAA Chemical Sciences Laboratory, Boulder, Colorado 80305, United States; Present Address: NOAA Global Monitoring Laboratory, Boulder, Colorado 80305, United States (J.P.);

  orcid.org/0000-0002-9320-7101
- Ilana Pollack Cooperative Institute for Research in Environmental Sciences, University of Colorado Boulder, Boulder, Colorado 80309, United States; NOAA Chemical Sciences Laboratory, Boulder, Colorado 80305, United States
- Michael A. Robinson Cooperative Institute for Research in Environmental Sciences, University of Colorado Boulder, Boulder, Colorado 80309, United States; NOAA Chemical Sciences Laboratory, Boulder, Colorado 80305, United States
- Andrew Rollins NOAA Chemical Sciences Laboratory, Boulder, Colorado 80305, United States
- Nell B. Schafer Cooperative Institute for Research in Environmental Sciences and Department of Chemistry, University of Colorado Boulder, Boulder, Colorado 80309, United States; NOAA Chemical Sciences Laboratory, Boulder, Colorado 80305, United States
- Rebecca H. Schwantes NOAA Chemical Sciences Laboratory, Boulder, Colorado 80305, United States; orcid.org/0000-0002-7095-3718
- Morgan Selby Cooperative Institute for Research in Environmental Sciences, University of Colorado Boulder, Boulder, Colorado 80309, United States; NOAA Chemical Sciences Laboratory, Boulder, Colorado 80305, United States; Present Address: Department of Chemistry, Colorado State University, Fort Collins, Colorado 80523, United States (M.S.); orcid.org/0009-0007-9259-9960
- Aaron Stainsby Institute of Climate and Energy Systems, ICE-3: Troposphere, Forschungszentrum Jülich, Jülich 52428, Germany
- Chelsea Stockwell NOAA Chemical Sciences Laboratory, Boulder, Colorado 80305, United States; ⊚ orcid.org/0000-0003-3462-2126

- Rose Taylor Chemical, Biochemical and Environmental Engineering, University of Maryland Baltimore County, Baltimore, Maryland 21250, United States; Present Address: Maryland Department of the Environment, Baltimore, Maryland 21230, United States (R.T.); orcid.org/0000-0003-1973-4613
- Victoria Treadaway Cooperative Institute for Research in Environmental Sciences, University of Colorado Boulder, Boulder, Colorado 80309, United States; NOAA Chemical Sciences Laboratory, Boulder, Colorado 80305, United States; Present Address: Colorado Department of Public Health and Environment, Air Pollution Control Division/ Technical Services Program, Denver, Colorado 80246, United States (V.T.)
- Patrick R. Veres NSF NCAR Earth Observing Laboratory, Boulder, Colorado 80307, United States
- Carsten Warneke NOAA Chemical Sciences Laboratory, Boulder, Colorado 80305, United States; orcid.org/0000-0003-3811-8496
- Eleanor Waxman Cooperative Institute for Research in Environmental Sciences, University of Colorado Boulder, Boulder, Colorado 80309, United States; NOAA Chemical Sciences Laboratory, Boulder, Colorado 80305, United States; orcid.org/0000-0001-5045-8149
- Paul O. Wennberg Division of Geological and Planetary Sciences and Division of Engineering and Applied Science, California Institute of Technology, Pasadena, California 91125, United States; Occid.org/0000-0002-6126-3854
- Glenn M. Wolfe Atmospheric Chemistry and Dynamics Lab, NASA Goddard Space Flight Center, Greenbelt, Maryland 20771, United States; Ocid.org/0000-0001-6586-4043
- Lu Xu Cooperative Institute for Research in Environmental Sciences, University of Colorado Boulder, Boulder, Colorado 80309, United States; NOAA Chemical Sciences Laboratory, Boulder, Colorado 80305, United States; Present Address: Department of Energy, Environmental, and Chemical Engineering, Washington University in St. Louis, St. Louis, Missouri 63130, United States (L.X.); orcid.org/0000-0002-0021-9876
- Kristen Zuraski Cooperative Institute for Research in Environmental Sciences, University of Colorado Boulder, Boulder, Colorado 80309, United States; NOAA Chemical Sciences Laboratory, Boulder, Colorado 80305, United States; orcid.org/0000-0003-3149-6611

Complete contact information is available at: https://pubs.acs.org/10.1021/acs.est.5c02073

#### **Notes**

The authors declare no competing financial interest.

## ACKNOWLEDGMENTS

The authors acknowledge the NOAA NESDIS Geostationary Extended Observations (GeoXO) Program for its support of AEROMMA flight operations. W.S.C., K.H.B., C.M.J., J.P., I.P., M.A.R., N.B.S., M.S., V.T., E.W., L.X., and K.Z. were partially supported by the NOAA Cooperative Agreement with CIRES, NA22OAR4320151. W.S.C. also received support from the University of Colorado Boulder Marion L. Sharrah Fellowship. G.I.G. was supported by the Klaus Tschira Boost Fund, a joint initiative of the German Scholars Organization and the Klaus Tschira Stiftung (grant no. KT28), and the European Research Council (ERC) under the European Union's Horizon 2022

research and innovation program (Grant agreement No. 101076276). G.M.W. acknowledges support from NOAA AC4 grant NA21OAR4310138-T1-01 and the NASA Tropospheric Composition program.

# REFERENCES

- (1) United Nations Department of Economic and Social Affairs. **2019**. *World Urbanization Prospects: The 2018 Revision*. New York.
- (2) Pozzer, A.; Anenberg, S. C.; Dey, S.; Haines, A.; Lelieveld, J.; Chowdhury, S. Mortality Attributable to Ambient Air Pollution: A Review of Global Estimates. *Geohealth* **2023**, *7*, No. e2022GH000711.
- (3) Huang, W.; Xu, H.; Wu, J.; Ren, M.; Ke, Y.; Qiao, J. Toward cleaner air and better health: Current state, challenges, and priorities. *Science* **2024**, *385*, *386*–*390*.
- (4) Duncan, B. N.; Lamsal, L. N.; Thompson, A. M.; Yoshida, Y.; Lu, Z.; Streets, D. G.; Hurwitz, M. M.; Pickering, K. E. A space-based, high-resolution view of notable changes in urban NOx pollution around the world (2005–2014). *Journal of Geophysical Research: Atmospheres* **2016**, 121 (2), 976–996.
- (5) Hassler, B.; McDonald, B. C.; Frost, G. J.; Borbon, A.; Carslaw, D. C.; Civerolo, K.; Granier, C.; Monks, P. S.; Monks, S.; Parrish, D. D.; Pollack, I. B.; Rosenlof, K. H.; Ryerson, T. B.; von Schneidemesser, E.; Trainer, M. Analysis of long-term observations of NOx and CO in megacities and application to constraining emissions inventories. *Geophys. Res. Lett.* **2016**, *43* (18), 9920–9930.
- (6) United States Environmental Protection Agency Air Pollutant Emissions Trends Data: National Tier 1 Criteria Air Pollutant Trends. https://www.epa.gov/air-emissions-inventories/air-pollutant-emissions-trends-data (accessed 1 February 2025).
- (7) Kim, S.-W.; McDonald, B. C.; Seo, S.; Kim, K. M.; Trainer, M. Understanding the Paths of Surface Ozone Abatement in the Los Angeles Basin. *J. Geophys. Res.: Atmos.* **2022**, 127 (4), No. e2021JD035606.
- (8) Warneke, C.; de Gouw, J. A.; Holloway, J. S.; Peischl, J.; Ryerson, T. B.; Atlas, E.; Blake, D.; Trainer, M.; Parrish, D. D. Multiyear trends in volatile organic compounds in Los Angeles, California: Five decades of decreasing emissions. *J. Geophys. Res.: Atmos.* **2012**, *117* (D21), D00V17.
- (9) Gu, S.; Guenther, A.; Faiola, C. Effects of Anthropogenic and Biogenic Volatile Organic Compounds on Los Angeles Air Quality. *Environ. Sci. Technol.* **2021**, *55* (18), 12191–12201.
- (10) Schlaerth, H. L.; Silva, S. J.; Li, Y. Characterizing Ozone Sensitivity to Urban Greening in Los Angeles Under Current Day and Future Anthropogenic Emissions Scenarios. *J. Geophys. Res.: Atmos.* **2023**, 128 (20), No. e2023JD039199.
- (11) Chen, X.; Millet, D. B.; Singh, H. B.; Wisthaler, A.; Apel, E. C.; Atlas, E. L.; Blake, D. R.; Bourgeois, I.; Brown, S. S.; Crounse, J. D.; de Gouw, J. A.; Flocke, F. M.; Fried, A.; Heikes, B. G.; Hornbrook, R. S.; Mikoviny, T.; Min, K. E.; Muller, M.; Neuman, J. A.; O'Sullivan, D. W.; Peischl, J.; Pfister, G. G.; Richter, D.; Roberts, J. M.; Ryerson, T. B.; Shertz, S. R.; Thompson, C. R.; Treadaway, V.; Veres, P. R.; Walega, J.; Warneke, C.; Washenfelder, R. A.; Weibring, P.; Yuan, B. On the sources and sinks of atmospheric VOCs: an integrated analysis of recent aircraft campaigns over North America. *Atmospheric Chemistry and Physics* **2019**, *19* (14), 9097–9123.
- (12) McDonald, B. C.; de Gouw, J. A.; Gilman, J. B.; Jathar, S. H.; Akherati, A.; Cappa, C. D.; Jimenez, J. L.; Lee-Taylor, J.; Hayes, P. L.; McKeen, S. A.; Cui, Y. Y.; Kim, S.-W.; Gentner, D. R.; Isaacman-VanWertz, G.; Goldstein, A. H.; Harley, R. A.; Frost, G. J.; Roberts, J. M.; Ryerson, T. B.; Trainer, M. Volatile chemical products emerging as largest petrochemical source of urban organic emissions. *Science* 2018, 359, 760–764.
- (13) Seltzer, K. M.; Murphy, B. N.; Pennington, E. A.; Allen, C.; Talgo, K.; Pye, H. O. T. Volatile Chemical Product Enhancements to Criteria Pollutants in the United States. *Environ. Sci. Technol.* **2022**, *56* (11), 6905–6913.
- (14) Coggon, M. M.; Stockwell, C. E.; Xu, L.; Peischl, J.; Gilman, J. B.; Lamplugh, A.; Bowman, H. J.; Aikin, K.; Harkins, C.; Zhu, Q.;

- Schwantes, R. H.; He, J.; Li, M.; Seltzer, K.; McDonald, B.; Warneke, C. Contribution of cooking emissions to the urban volatile organic compounds in Las Vegas. *NV. Atmospheric Chemistry and Physics* **2024**, 24 (7), 4289–4304.
- (15) Li, J.; Qin, Y.; Zhang, X.; Shan, B.; Liu, C. Emission Characteristics, Environmental Impacts, and Health Risks of Volatile Organic Compounds from Asphalt Materials: A State-of-the-Art Review. *Energy Fuels* **2024**, *38* (6), 4787–4802.
- (16) Coggon, M. M.; Gkatzelis, G. I.; McDonald, B. C.; Gilman, J. B.; Schwantes, R. H.; Abuhassan, N.; Aikin, K. C.; Arend, M. F.; Berkoff, T. A.; Brown, S. S.; Campos, T. L.; Dickerson, R. R.; Gronoff, G.; Hurley, J. F.; Isaacman-VanWertz, G.; Koss, A. R.; Li, M.; McKeen, S. A.; Moshary, F.; Peischl, J.; Pospisilova, V.; Ren, X.; Wilson, A.; Wu, Y.; Trainer, M.; Warneke, C. Volatile chemical product emissions enhance ozone and modulate urban chemistry. *Proc. Natl. Acad. Sci. U. S. A.* **2021**, *118* (32), No. e2026653118.
- (17) McDuffie, E. E.; Edwards, P. M.; Gilman, J. B.; Lerner, B. M.; Dubé, W. P.; Trainer, M.; Wolfe, D. E.; Angevine, W. M.; de Gouw, J.; Williams, E. J.; Tevlin, A. G.; Murphy, J. G.; Fischer, E. V.; McKeen, S.; Ryerson, T. B.; Peischl, J.; Holloway, J. S.; Aikin, K.; Langford, A. O.; Senff, C. J.; Alvarez, R. J.; Hall, S. R.; Ullmann, K.; Lantz, K. O.; Brown, S. S. Influence of oil and gas emissions on summertime ozone in the Colorado Northern Front Range. *Journal of Geophysical Research: Atmospheres* **2016**, *121* (14), 8712–8729.
- (18) Chang, C.-Y.; Faust, E.; Hou, X.; Lee, P.; Kim, H. C.; Hedquist, B. C.; Liao, K.-J. Investigating ambient ozone formation regimes in neighboring cities of shale plays in the Northeast United States using photochemical modeling and satellite retrievals. *Atmos. Environ.* **2016**, 142, 152–170.
- (19) Pozzer, A.; Schultz, M. G.; Helmig, D. Impact of U.S. Oil and Natural Gas Emission Increases on Surface Ozone Is Most Pronounced in the Central United States. *Environ. Sci. Technol.* **2020**, *54* (19), 12423–12433.
- (20) Roohani, Y. H.; Roy, A. A.; Heo, J.; Robinson, A. L.; Adams, P. J. Impact of natural gas development in the Marcellus and Utica shales on regional ozone and fine particulate matter levels. *Atmos. Environ.* **2017**, 155, 11–20.
- (21) Rickly, P. S.; Coggon, M. M.; Aikin, K. C.; Alvarez, R. J., 2nd; Baidar, S.; Gilman, J. B.; Gkatzelis, G. I.; Harkins, C.; He, J.; Lamplugh, A.; Langford, A. O.; McDonald, B. C.; Peischl, J.; Robinson, M. A.; Rollins, A. W.; Schwantes, R. H.; Senff, C. J.; Warneke, C.; Brown, S. S. Influence of Wildfire on Urban Ozone: An Observationally Constrained Box Modeling Study at a Site in the Colorado Front Range. *Environ. Sci. Technol.* 2023, 57 (3), 1257–1267.
- (22) Langford, A. O.; Senff, C. J.; Alvarez, R. J.; Aikin, K. C.; Ahmadov, R.; Angevine, W. M.; Baidar, S.; Brewer, W. A.; Brown, S. S.; James, E. P.; McCarty, B. J.; Sandberg, S. P.; Zucker, M. L. Were Wildfires Responsible for the Unusually High Surface Ozone in Colorado During 2021? *J. Geophys. Res.: Atmos.* 2023, 128 (12), No. e2022JD037700.
- (23) Brey, S. J.; Fischer, E. V. Smoke in the City: How Often and Where Does Smoke Impact Summertime Ozone in the United States? *Environ. Sci. Technol.* **2016**, *50* (3), 1288–94.
- (24) Jaffe, D. A.; O'Neill, S. M.; Larkin, N. K.; Holder, A. L.; Peterson, D. L.; Halofsky, J. E.; Rappold, A. G. Wildfire and prescribed burning impacts on air quality in the United States. *J. Air Waste Manage. Assoc.* **2020**, 70 (6), 583–615.
- (25) Chameides, W. L. The photochemical role of tropospheric nitrogen oxides. *Geophys. Res. Lett.* **1978**, *5* (1), 17–20.
- (26) Crutzen, P. J. The role of NO and NO<sub>2</sub> in the chemistry of the troposphere and stratosphere. *Annu. Rev. Earth Planet. Sci.* **1979**, 7, 443–472.
- (27) Seinfeld, J. H. Urban Air Pollution: The State of the Science. *Science* **1989**, 243, 745–752.
- (28) Liu, S. C.; Trainer, M.; Fehsenfeld, F. C.; Parrish, D. D.; Williams, E. J.; Fahey, D. W.; Hubler, G.; Murphy, P. C. Ozone production in the rural troposphere and the implications for regional and global ozone distributions. *Journal of Geophysical Research: Atmospheres* 1987, 92 (D4), 4191–4207.

- (29) Trainer, M.; Parrish, D. D.; Buhr, M. P.; Norton, R. B.; Fehsenfeld, F. C.; Anlauf, K. G.; Bottenheim, J. W.; Tang, Y. Z.; Wiebe, H. A.; Roberts, J. M.; Tanner, R. L.; Newman, L.; Bowersox, V. C.; Meagher, J. F.; Olszyna, K. J.; Rodgers, M. O.; Wang, T.; Berresheim, H.; Demerjian, K. L.; Roychowdhury, U. K. Correlation of ozone with NO<sub>y</sub> in photochemically aged air. *Journal of Geophysical Research: Atmospheres* 1993, 98 (D2), 2917–2925.
- (30) Ryerson, T. B.; Trainer, M.; Holloway, J.; Parrish, D. D.; Huey, L. G.; Sueper, D. T.; Frost, G. J.; Donnelly, S. G.; Schauffler, S.; Atlas, E.; Kuster, W. C.; Goldan, P. D.; Hubler, G.; Meagher, J. F.; Fehsenfeld, F. C. Observations of Ozone Formation in Power Plant Plumes and Implications for Ozone Control Strategies. *Science* 2001, 292, 719–723.
- (31) St. John, J. C.; Chameides, W. L.; Saylor, R. Role of anthropogenic NO<sub>x</sub> and VOC as ozone precursors: A case study from the SOS Nashville/Middle Tennessee Ozone Study. *J. Geophys. Res.: Atmos.* **1998**, *103* (D17), 22415–22423.
- (32) Kleinman, L. I.; Daum, P. H.; Lee, Y.; Nunnermacker, L. J.; Springston, S. R.; Weinstein-Lloyd, J.; Rudolph, J. Ozone production efficiency in an urban area. *J. Geophys. Res.: Atmos.* **2002**, *107* (D23), ACH23–1–ACH 23–12.
- (33) Zaveri, R. A.; Berkowitz, C. M.; Kleinman, L. I.; Springston, S. R.; Doskey, P. V.; Lonneman, W. A.; Spicer, C. W. Ozone production efficiency and NOx depletion in an urban plume: Interpretation of field observations and implications for evaluating O3-NOx-VOC sensitivity. *J. Geophys. Res.: Atmos.* **2003**, *108* (D14), ACH-12-1-ACH-12-23.
- (34) Lin, X.; Trainer, M.; Liu, S. C. On the nonlinearity of the tropospheric ozone production. *Journal of Geophysical Research* 1988, 93 (D12), 15879–15888.
- (35) Griffin, R. J.; Revelle, M. K.; Dabdub, D. Modeling the Oxidative Capacity of the Atmosphere of the South Coast Air Basin of California. 1. Ozone Formation Metrics. *Environ. Sci. Technol.* **2004**, *38* (3), 746–752.
- (36) Sillman, S.; He, D. Some theoretical results concerning O3-NOx-VOC chemistry and NOx-VOC indicators. *J. Geophys. Res.: Atmos.* **2002**, *107* (D22), ACH-26–1–ACH-26–15.
- (37) Schroeder, J. R.; Crawford, J. H.; Fried, A.; Walega, J.; Weinheimer, A.; Wisthaler, A.; Müller, M.; Mikoviny, T.; Chen, G.; Shook, M.; Blake, D. R.; Tonnesen, G. S. New insights into the column CH2O/NO2 ratio as an indicator of near-surface ozone sensitivity. *Journal of Geophysical Research: Atmospheres* **2017**, 122 (16), 8885–8907.
- (38) Sebol, A. E.; Canty, T. P.; Wolfe, G. M.; Hannun, R.; Ring, A. M.; Ren, X. Exploring ozone production sensitivity to NOx and VOCs in the New York City airshed in the spring and summers of 2017–2019. *Atmos. Environ.* **2024**, 324, No. 120417.
- (39) Wang, J.; Ge, B.; Wang, Z. Ozone Production Efficiency in Highly Polluted Environments. *Current Pollution Reports* **2018**, 4 (3), 198–207.
- (40) Ryerson, T. B.; Buhr, M. P.; Frost, G. J.; Goldan, P. D.; Holloway, J. S.; Hübler, G.; Jobson, B. T.; Kuster, W. C.; McKeen, S. A.; Parrish, D. D.; Roberts, J. M.; Sueper, D. T.; Trainer, M.; Williams, J.; Fehsenfeld, F. C. Emissions lifetimes and ozone formation in power plant plumes. *Journal of Geophysical Research: Atmospheres* 1998, 103 (D17), 22569–22583.
- (41) Pollack, I. B.; Ryerson, T. B.; Trainer, M.; Parrish, D. D.; Andrews, A. E.; Atlas, E. L.; Blake, D. R.; Brown, S. S.; Commane, R.; Daube, B. C.; de Gouw, J. A.; Dubé, W. P.; Flynn, J.; Frost, G. J.; Gilman, J. B.; Grossberg, N.; Holloway, J. S.; Kofler, J.; Kort, E. A.; Kuster, W. C.; Lang, P. M.; Lefer, B.; Lueb, R. A.; Neuman, J. A.; Nowak, J. B.; Novelli, P. C.; Peischl, J.; Perring, A. E.; Roberts, J. M.; Santoni, G.; Schwarz, J. P.; Spackman, J. R.; Wagner, N. L.; Warneke, C.; Washenfelder, R. A.; Wofsy, S. C.; Xiang, B. Airborne and ground-based observations of a weekend effect in ozone, precursors, and oxidation products in the California South Coast Air Basin. *J. Geophys. Res.: Atmos.* 2012, 117 (D21), D00V05.
- (42) Rickard, A. R.; Salisbury, G.; Monks, P. S.; Lewis, A. C.; Baugitte, S.; Bandy, B. J.; Clemitshaw, K. C.; Penkett, S. A. Comparison of measured ozone production efficiencies in the marine boundary layer at

- two European coastal sites under different pollution regimes. *J. Atmos Chem.* **2002**, 43, 107–134.
- (43) Ninneman, M.; Demerjian, K. L.; Schwab, J. J. Ozone Production Efficiencies at Rural New York State Locations: Relationship to Oxides of Nitrogen Concentrations. *Journal of Geophysical Research: Atmospheres* **2019**, *124* (4), 2363–2376.
- (44) Fujita, E. M.; Campbell, D. E.; Stockwell, W. R.; Saunders, E.; Fitzgerald, R.; Perea, R. Projected ozone trends and changes in the ozone-precursor relationship in the South Coast Air Basin in response to varying reductions of precursor emissions. *J. Air Waste Manage. Assoc.* **2016**, *66* (2), 201–214.
- (45) Mazzuca, G. M.; Ren, X.; Loughner, C. P.; Estes, M.; Crawford, J. H.; Pickering, K. E.; Weinheimer, A. J.; Dickerson, R. R. Ozone production and its sensitivity to  $NO_x$  and VOCs: results from the DISCOVER-AQ field experiment, Houston 2013. *Atmospheric Chemistry and Physics* **2016**, 16 (22), 14463–14474.
- (46) Ninneman, M.; Lu, S.; Lee, P.; McQueen, J.; Huang, J.; Demerjian, K.; Schwab, J. Observed and Model-Derived Ozone Production Efficiency over Urban and Rural New York State. *Atmosphere* **2017**, *8* (7), 126.
- (47) Yang, Y.; Shao, M.; Keßel, S.; Li, Y.; Lu, K.; Lu, S.; Williams, J.; Zhang, Y.; Zeng, L.; Nölscher, A. C.; Wu, Y.; Wang, X.; Zheng, J. How the OH reactivity affects the ozone production efficiency: case studies in Beijing and Heshan. *China. Atmospheric Chemistry and Physics* **2017**, 17 (11), 7127–7142.
- (48) Zhou, W.; Cohan, D. S.; Henderson, B. H. Slower ozone production in Houston, Texas following emission reductions: evidence from Texas Air Quality Studies in 2000 and 2006. *Atmospheric Chemistry and Physics* **2014**, *14* (6), 2777–2788.
- (49) Tran, T.; Kumar, N.; Knipping, E. Investigating sensitivity of ozone to emission reductions in the New York City (NYC) metropolitan and downwind areas. *Atmos. Environ.* **2023**, 301, No. 119675.
- (50) Li, L.; Li, J.; Qin, M.; Xie, X.; Hu, J.; Zhang, Y. Variations in summertime ozone in Nanjing between 2015 and 2020: roles of meteorology, radical chain length and ozone production efficiency. *Front. Environ. Sci. Eng.* **2024**, *18* (11), 137.
- (51) Pollack, I. B.; Ryerson, T. B.; Trainer, M.; Neuman, J. A.; Roberts, J. M.; Parrish, D. D. Trends in ozone, its precursors, and related secondary oxidation products in Los Angeles, California: A synthesis of measurements from 1960 to 2010. *Journal of Geophysical Research: Atmospheres* **2013**, *118* (11), 5893–5911.
- (52) Oak, Y. J.; Park, R. J.; Schroeder, J. R.; Crawford, J. H.; Blake, D. R.; Weinheimer, A. J.; Woo, J. H.; Kim, S. W.; Yeo, H.; Fried, A.; Wisthaler, A.; Brune, W. H.; Helmig, D.; Stutz, J. Evaluation of simulated  $O_3$  production efficiency during the KORUS-AQ campaign: Implications for anthropogenic  $NO_x$  emissions in Korea. *Elementa: Sci. Anthropocene* **2019**, 7 (56), 1–15.
- (53) Zoogman, P.; Liu, X.; Suleiman, R. M.; Pennington, W. F.; Flittner, D. E.; Al-Saadi, J. A.; Hilton, B. B.; Nicks, D. K.; Newchurch, M. J.; Carr, J. L.; Janz, S. J.; Andraschko, M. R.; Arola, A.; Baker, B. D.; Canova, B. P.; Chan Miller, C.; Cohen, R. C.; Davis, J. E.; Dussault, M. E.; Edwards, D. P.; Fishman, J.; Ghulam, A.; Gonzalez Abad, G.; Grutter, M.; Herman, J. R.; Houck, J.; Jacob, D. J.; Joiner, J.; Kerridge, B. J.; Kim, J.; Krotkov, N. A.; Lamsal, L.; Li, C.; Lindfors, A.; Martin, R. V.; McElroy, C. T.; McLinden, C.; Natraj, V.; Neil, D. O.; Nowlan, C. R.; O'Sullivan, E. J.; Palmer, P. I.; Pierce, R. B.; Pippin, M. R.; Saiz-Lopez, A.; Spurr, R. J. D.; Szykman, J. J.; Torres, O.; Veefkind, J. P.; Veihelmann, B.; Wang, H.; Wang, J.; Chance, K. Tropospheric Emissions: Monitoring of Pollution (TEMPO). J. Quant. Spectrosc. Radiat. Transfer 2017, 186, 17–39.
- (54) United States Census Bureau. Annual Estimates of the Resident Population for Metropolitan Statistical Areas in the United States and Puerto Rico: April 1, 2020 to July 1, 2023, https://www.census.gov/data/datasets/time-series/demo/popest/2020s-total-metro-and-micro-statistical-areas.html (accessed 1 February 2025).
- (55) United States Environmental Protection Agency. *Our Nation's Air: Trends Through* 2023. https://gispub.epa.gov/air/trendsreport/2024 (accessed 1 February 2025).

- (56) Washenfelder, R. A.; Wagner, N. L.; Dube, W. P.; Brown, S. S. Measurement of atmospheric ozone by cavity ring-down spectroscopy. *Environ. Sci. Technol.* **2011**, 45 (7), 2938–44.
- (57) Wild, R. J.; Edwards, P. M.; Dube, W. P.; Baumann, K.; Edgerton, E. S.; Quinn, P. K.; Roberts, J. M.; Rollins, A. W.; Veres, P. R.; Warneke, C.; Williams, E. J.; Yuan, B.; Brown, S. S. A measurement of total reactive nitrogen, NO<sub>y</sub>, together with NO<sub>2</sub>, NO, and O<sub>3</sub> via cavity ringdown spectroscopy. *Environ. Sci. Technol.* **2014**, *48* (16), 9609–9615.
- (58) Bourgeois, I.; Peischl, J.; Thompson, C. R.; Aikin, K. C.; Campos, T.; Clark, H.; Commane, R.; Daube, B.; Diskin, G. W.; Elkins, J. W.; Gao, R.-S.; Gaudel, A.; Hintsa, E. J.; Johnson, B. J.; Kivi, R.; McKain, K.; Moore, F. L.; Parrish, D. D.; Querel, R.; Ray, E.; Sánchez, R.; Sweeney, C.; Tarasick, D. W.; Thompson, A. M.; Thouret, V.; Witte, J. C.; Wofsy, S. C.; Ryerson, T. B. Global-scale distribution of ozone in the remote troposphere from the ATom and HIPPO airborne field missions. *Atmospheric Chemistry and Physics* **2020**, *20* (17), 10611–10635.
- (59) Rollins, A. W.; Rickly, P. S.; Gao, R.-S.; Ryerson, T. B.; Brown, S. S.; Peischl, J.; Bourgeois, I. Single-photon laser-induced fluorescence detection of nitric oxide at sub-parts-per-trillion mixing ratios. *Atmospheric Measurement Techniques* **2020**, *13* (5), 2425–2439.
- (60) Ryerson, T. B.; Huey, L. G.; Knapp, K.; Neuman, J. A.; Parrish, D. D.; Sueper, D. T.; Fehsenfeld, F. C. Design and initial characterization of an inlet for gas-phase NO<sub>y</sub> measurements from aircraft. *Journal of Geophysical Research: Atmospheres* **1999**, *104* (D5), 5483–5492.
- (61) Neuman, J. A.; Nowak, J. B.; Zheng, W.; Flocke, F.; Ryerson, T. B.; Trainer, M.; Holloway, J. S.; Parrish, D. D.; Frost, G. J.; Peischl, J.; Atlas, E. L.; Bahreini, R.; Wollny, A. G.; Fehsenfeld, F. C. Relationship between photochemical ozone production and NO<sub>x</sub> oxidation in Houston, Texas. *J. Geophys. Res.: Atmos.* **2009**, *114* (D7), D00F08.
- (62) Boggs, P. T.; Spiegelman, C. H.; Donaldson, J. R.; Schnabel, R. B. A Computational Examination of Orthogonal Distance Regression. *Journal of Econometrics* **1988**, 38, 169–201.
- (63) Wu, C.; Yu, J. Z. Evaluation of linear regression techniques for atmospheric applications: the importance of appropriate weighting. *Atmospheric Measurement Techniques* **2018**, *11* (2), 1233–1250.
- (64) Wolfe, G. M.; Marvin, M. R.; Roberts, S. J.; Travis, K. R.; Liao, J. The Framework for 0-D Atmospheric Modeling (F0AM) v3.1. Geoscientific Model Development 2016, 9 (9), 3309–3319.
- (65) Jenkin, M. E.; Young, J. C.; Rickard, A. R. The MCM v3.3.1 degradation scheme for isoprene. *Atmospheric Chemistry and Physics* **2015**, *15* (20), 11433–11459.
- (66) Cohen, M. D.; Stunder, B. J. B.; Rolph, G. D.; Draxler, R. R.; Stein, A. F.; Ngan, F. NOAA's HYSPLIT Atmospheric Transport and Dispersion Modeling System. *Bulletin of the American Meteorological Society* **2015**, 96 (12), 2059–2077.
- (67) Lennartson, G. J.; Schwartz, M. D. The lake breeze—ground-level ozone connection in eastern Wisconsin: a climatological perspective. *International Journal of Climatology* **2002**, 22 (11), 1347–1364.
- (68) Sullivan, J. T.; Berkoff, T.; Gronoff, G.; Knepp, T.; Pippin, M.; Allen, D.; Twigg, L.; Swap, R.; Tzortziou, M.; Thompson, A. M.; Stauffer, R. M.; Wolfe, G. M.; Flynn, J.; Pusede, S. E.; Judd, L.; Moore, W.; Baker, B. D.; Al-Saadi, J.; McGee, T. J. The Ozone Water-Land Environmental Transition Study (OWLETS): An Innovative Strategy for Understanding Chesapeake Bay Pollution Events. *Bulletin of the American Meteorological Society* 2019, 100 (2), 291–306.
- (69) Zhang, J.; Catena, A.; Shrestha, B.; Freedman, J.; McCabe, E.; Schwab, M. J.; Felton, D.; Kent, J.; Gaza, B.; Schwab, J. J. Unraveling the interaction of urban emission plumes and marine breezes involved in the formation of summertime coastal high ozone on Long Island. *Environmental Science: Atmospheres* **2022**, *2* (6), 1438–1449.
- (70) Northeast States for Coordinated Air Use Management **2017**. Retrospective and Future Analysis of Air Quality In and Downwind of New York City.
- (71) Torres-Vazquez, A.; Pleim, J.; Gilliam, R.; Pouliot, G. Performance Evaluation of the Meteorology and Air Quality Conditions From Multiscale WRF-CMAQ Simulations for the Long Island Sound Tropospheric Ozone Study (LISTOS). *J. Geophys. Res.: Atmos.* **2022**, 127 (5), No. e2021JD035890.

- (72) Cleary, P. A.; Dickens, A.; McIlquham, M.; Sanchez, M.; Geib, K.; Hedberg, C.; Hupy, J.; Watson, M. W.; Fuoco, M.; Olson, E. R.; Pierce, R. B.; Stanier, C.; Long, R.; Valin, L.; Conley, S.; Smith, M. Impacts of lake breeze meteorology on ozone gradient observations along Lake Michigan Shorelines in Wisconsin. *Atmos. Environ.* **2022**, 269, No. 118834.
- (73) Fast, J. D.; Heilman, W. E. The Effect of Lake Temperatures and Emissions on Ozone Exposure in the Western Great Lakes Region. *Journal of Applied Meteorology* **2003**, 42, 1197–1217.
- (74) Fast, J. D.; Heilman, W. E. Simulated sensitivity of seasonal ozone exposure in the Great Lakes region to changes in anthropogenic emissions in the presence of interannual variability. *Atmos. Environ.* **2005**, 39 (29), 5291–5306.
- (75) Vermeuel, M. P.; Novak, G. A.; Alwe, H. D.; Hughes, D. D.; Kaleel, R.; Dickens, A. F.; Kenski, D.; Czarnetzki, A. C.; Stone, E. A.; Stanier, C. O.; Pierce, R. B.; Millet, D. B.; Bertram, T. H. Sensitivity of Ozone Production to NO<sub>x</sub> and VOC Along the Lake Michigan Coastline. *Journal of Geophysical Research: Atmospheres* **2019**, *124* (20), 10989–11006.
- (76) Abdi-Oskouei, M.; Roozitalab, B.; Stanier, C. O.; Christiansen, M.; Pfister, G.; Pierce, R. B.; McDonald, B. C.; Adelman, Z.; Janseen, M.; Dickens, A. F.; Carmichael, G. R. The Impact of Volatile Chemical Products Other VOCs, and NOx on Peak Ozone in the Lake Michigan Region. *J. Geophys. Res.: Atmos.* **2022**, 127 (22), No. e2022JD037042.
- (77) Lu, R.; Turco, L. P. Air pollutant transport in a coastal environment II. Three-dimensional simulations over Los Angeles Basin. *Atmos. Environ.* **1995**, 29 (13), 1499–1518.
- (78) California Air Resources Board Appendix B: South Coast Air Basin Ozone Weight of Evidence Analysis 2023
- (79) Nussbaumer, C. M.; Cohen, R. C. The Role of Temperature and  $NO_x$  in Ozone Trends in the Los Angeles Basin. *Environ. Sci. Technol.* **2020**, *54* (24), 15652–15659.
- (80) Perdigones, B. C.; Lee, S.; Cohen, R. C.; Park, J. H.; Min, K. E. Two Decades of Changes in Summertime Ozone Production in California's South Coast Air Basin. *Environ. Sci. Technol.* **2022**, *56* (15), 10586–10595.
- (81) Stockwell, C. E.; Coggon, M. M.; Schwantes, R. H.; Harkins, C.; Verreyken, B.; Lyu, C.; Zhu, Q.; Xu, L.; Gilman, J. B.; Lamplugh, A.; Peischl, J.; Robinson, M. A.; Veres, P. R.; Li, M.; Rollins, A. W.; Zuraski, K.; Baidar, S.; Liu, S.; Kuwayama, T.; Brown, S. S.; McDonald, B. C.; Warneke, C. Urban ozone formation and sensitivities to volatile chemical products, cooking emissions, and NO<sub>x</sub> upwind of and within two Los Angeles Basin cities. *Atmospheric Chemistry and Physics* **2025**, 25 (2), 1121–1143.
- (82) Wu, S.; Alaimo, C. P.; Zhao, Y.; Green, P. G.; Young, T. M.; Liu, S.; Kuwayama, T.; Coggon, M. M.; Stockwell, C. E.; Xu, L.; Warneke, C.; Gilman, J. B.; Robinson, M. A.; Veres, P. R.; Neuman, J. A.; Kleeman, M. J. O<sub>3</sub> Sensitivity to NO<sub>x</sub> and VOC During RECAP-CA: Implication for Emissions Control Strategies. *ACS ES&T Air* 2024, *1* (6), 536–546.
- (83) Sillman, S. Ozone production efficiency and loss of  $NO_x$  in power plant plumes: Photochemical model and interpretation of measurements in Tennessee. *Journal of Geophysical Research: Atmospheres* **2000**, 105 (D7), 9189–9202.
- (84) Blanchard, C. L.; Hidy, G. M. Ozone response to emission reductions in the southeastern United States. *Atmospheric Chemistry and Physics* **2018**, *18* (11), 8183–8202.
- (85) Fujita, E. M.; Campbell, D. E.; Zielinska, B.; Arnott, W. P.; Chow, J. C. Concentrations of air toxics in motor vehicle-dominated environments. *Res. Rep. Health Eff. Inst.* **2011**, 3–77.
- (86) Bolden, A. L.; Kwiatkowski, C. F.; Colborn, T. New Look at BTEX: Are Ambient Levels a Problem? *Environ. Sci. Technol.* **2015**, 49 (9), 5261–5276.
- (87) Gkatzelis, G. I.; Coggon, M. M.; McDonald, B. C.; Peischl, J.; Gilman, J. B.; Aikin, K. C.; Robinson, M. A.; Canonaco, F.; Prevot, A. S. H.; Trainer, M.; Warneke, C. Observations Confirm that Volatile Chemical Products Are a Major Source of Petrochemical Emissions in U.S. Cities. *Environmental Science & Technology* **2021**, *55* (8), 4332–4343.

- (88) Stainsby, A.; AEROMMA Team. Airborne Measurements of OH Reactivity over Urban Megacities. In *EGU General Assembly* 2024, Vienna, Austria, 2024.
- (89) United States Environmental Protection Agency. Air Pollutant Emissions Trends Data: State Tier 1 Criteria Air Pollutants Trends. https://www.epa.gov/air-emissions-inventories/air-pollutant-emissions-trends-data (accessed 1 February 2025).
- (90) Kleinman, L. I.; Daum, P. H.; Imre, D. G.; Lee, J. H.; Lee, Y. N.; Nunnermacker, L. J.; Springston, S. R.; Weinstein-Lloyd, J.; Newman, L. Ozone production in the New York City urban plume. *Journal of Geophysical Research: Atmospheres* **2000**, *105* (D11), 14495–14511.
- (91) Parker, H. A.; Hasheminassab, S.; Crounse, J. D.; Roehl, C. M.; Wennberg, P. O. Impacts of Traffic Reductions Associated With COVID-19 on Southern California Air Quality. *Geophys. Res. Lett.* **2020**, 47 (23), No. e2020GL090164.

